

Pairing of two vertical columnar vortices in a stratified fluid



Pantxika Otheguy^{a,b}, Jean-Marc Chomaz^a, Pierre Augier^{a,*}, Yoshifumi Kimura^{c,d}, Paul Billant^a

^a LadHyX, CNRS, École Polytechnique, F-91128 Palaiseau Cedex, France

^b Centre Technique Littoral, Lyonnaise des Eaux, Pavillon Izarbel, 64210 Bidart, France

^c Graduate School of Mathematics, Nagoya University, Furo-cho, Chikusa-ku, Nagoya 464-8602, Japan

^d National Center for Atmospheric Research, P.O. Box 3000, Boulder, CO 80307, USA

ARTICLE INFO

Article history:

Available online 2 June 2014

Keywords:

Stratification
Zigzag instability
Pairing of vortices
Wave generation

ABSTRACT

We present three-dimensional (3D) numerical simulations of the pairing of two vertical columnar vortices in a stably stratified fluid. Whereas in two dimensions, merging of two isolated vortices occurs on a diffusion time scale, in the three-dimensional stratified case we show that merging is a much faster process that occurs over an inertial time scale. The sequence of dynamical processes that leads to this accelerated pairing involves first a linear stage where the zigzag instability develops displacing vortices alternately closer and farther with a vertical periodicity scaling on the buoyancy length scale $L_B = F_h b$, where F_h is the horizontal Froude number ($F_h = \Gamma / \pi a^2 N$ with a the core size of the vortices, Γ their circulation and N the Brunt–Väisälä frequency) and b is the separation distance between the vortices. In layers where the vortices have started to move closer, their distance decreases exponentially with the growth rate of the zigzag instability. Non-linearities do not seem to affect this process and the decrease only stops when the pairing is completed in that layer. At the same time, enstrophy that has also grown exponentially reaches a magnitude of the order of the Reynolds number $Re = \Gamma / (\pi \nu)$ (where ν is the kinematic viscosity of the fluid) if the Reynolds number is not too large, meaning that energy is then dissipated on the inertial time scale. This dissipation occurs in thin layers and the vortices that were originally moving away in the intermediate layer start slowing down and rapidly merge.

© 2014 Elsevier Masson SAS. All rights reserved.

1. Introduction

Atmosphere, oceans and some astrophysical fluids are stably stratified (see [1] for a review) and rotating. At mesoscale for the Earth's atmosphere, i.e. between 1 and 100 km, the planetary rotation is weak and the stratification controls the dynamics. Nastrom, Gage and Jaspersen [2] reported that the kinetic energy spectrum versus horizontal wavenumber k_h is of the form $k_h^{-5/3}$ for the atmosphere in the mesoscale range, whereas it is of the form k_h^{-3} at larger scales. Following Lilly [3], they suggested that this $k_h^{-5/3}$ spectrum might be due to an inverse energy cascade from small (~ 1 km) to large (~ 500 km) scales, similar to the energy cascade

predicted for two-dimensional (2D) turbulence by Kraichnan [4] and well confirmed by numerical simulations and experiments. In 2D, energy is transferred by the merging of two vortices to form a larger one [5]. The idea that the potential vorticity in a stratified flow even at slow time scale in the absence of the gravity wave component might behave as a 2D fluid was questioned by many authors [6–10]. In particular, [11,12] showed that several 2D flows were unstable when the fluid is stratified, and they named this instability the zigzag instability. Specifically, the zigzag instability affects co-rotating vortex pairs [13,12] and has a growth rate which scales as twice the external strain field generated by one vortex on the other ($S = \Gamma / 2\pi b^2$). Thus, this instability is as fast as the rotation $\Omega = \Gamma / \pi b^2$ of the vortex pair. Destabilization should thus occur in a few rotations of the pair and as a consequence, this instability should strongly affect the merging between vortices, and may therefore help explaining the departure of the stratified turbulence from two-dimensional turbulence.

In the present paper, we investigate through numerical simulations a single pairing event in a strongly stratified fluid in order to find out to which extent stratification affects this

* Correspondence to: Department of Applied Mathematics and Theoretical Physics, University of Cambridge, Centre for Mathematical Sciences, Wilberforce Road, Cambridge CB3 0WA, UK.

E-mail addresses: pantxika.otheguy@ensta.org (P. Otheguy), pierre.augier@ens-lyon.org (P. Augier).

<http://dx.doi.org/10.1016/j.euromechflu.2014.05.007>

0997-7546/© 2014 Elsevier Masson SAS. All rights reserved.

process. In particular, we will compare this stratified merging to purely two-dimensional merging. The second section presents the numerical method used to study a pairing event by direct numerical simulations. The third section shows the qualitative behavior of the merging. The fourth, fifth and sixth sections describe and analyze in detail the pairing in a stratified fluid.

2. Numerical simulations

2.1. Governing equations and numerical method

The dynamics of the flow is governed by the incompressible Navier–Stokes equations under the Boussinesq approximation:

$$\frac{\partial \mathbf{u}}{\partial t} = \mathbf{u} \wedge \boldsymbol{\omega} - \nabla \left[p + \frac{\mathbf{u}^2}{2} \right] - \rho \mathbf{e}_z + \nu \Delta \mathbf{u}, \quad (1)$$

$$\frac{\partial \rho}{\partial t} + \mathbf{u} \cdot \nabla \rho = N^2 u_z + D \Delta \rho \quad (2)$$

where \mathbf{e}_z is the unit vector in the z -direction pointing upward, p the pressure field, \mathbf{u} the non-divergent velocity ($\text{div } \mathbf{u} = 0$), $u_z = \mathbf{e}_z \cdot \mathbf{u}$ its vertical component, D the diffusivity of the stratifying agent and ν the kinematic viscosity. The density field is the sum of a constant density ρ_0 , a linear profile $\bar{\rho}(z)$ and a perturbation $\rho_0 \rho/g$. The density perturbation is rescaled by g/ρ_0 in order to avoid an extra constant in Eq. (1). The Brunt–Väisälä frequency is $N = \sqrt{-(g/\rho_0) d\bar{\rho}/dz}$, where g is the gravity acceleration.

Eqs. (1)–(2) are expressed in the Fourier space:

$$\frac{d\hat{\mathbf{u}}}{dt} = P(\mathbf{k}) [\widehat{\mathbf{u} \wedge \boldsymbol{\omega}} - \hat{\rho} \mathbf{e}_z] - \nu \mathbf{k}^2 \hat{\mathbf{u}}, \quad (3)$$

$$\frac{d\hat{\rho}}{dt} = N^2 \hat{u}_z - D \mathbf{k}^2 \hat{\rho}, \quad (4)$$

where the Fourier transform is denoted by a hat, \mathbf{k} is the wavenumber and $P(\mathbf{k})$ is the projection operator on the solenoidal space. To compute (3)–(4), we use a pseudo-spectral solver adapted from the unstratified code used by [14]. The computational domain is a parallelepipedic box of height L_z with a square horizontal base ($L_x = L_y$ where L_x and L_y are the dimensions respectively in the x and y directions). The spatial resolution is chosen to be about the same in all directions implying that the numbers of collocation points on the horizontal directions are equal, $n_x = n_y$, and that the number of collocation points on the vertical is $n_z \sim n_x L_z / L_x$. Time integration is performed with a second order Adams–Bashforth scheme. Dissipative terms are integrated exactly. The 2/3 rule is applied for de-aliasing.

2.2. Initial conditions

The initial velocity field \mathbf{U} is made of a quasi-steady 2D pair of co-rotating vortices $\mathbf{U}_{2D}(x, y)$ perturbed by the most unstable 3D eigenmode \mathbf{U}'

$$\mathbf{U}(x, y, z, t = 0) = \mathbf{U}_{2D}(x, y) + A \Re(e^{ik_{zm}z} \mathbf{U}'(x, y)) \quad (5)$$

where A is the amplitude of the perturbation, \Re denotes the real part and k_{zm} is the most unstable vertical wavenumber obtained by a linear stability analysis [13]. In most simulations, the vertical size of the box L_z is set to the most unstable wavelength $L_z = \lambda_{max} = 2\pi/k_{zm}$.

In order to obtain the basic flow \mathbf{U}_{2D} , a 2D non-linear simulation is first carried out with the following initial vorticity field corresponding to two identical co-rotating gaussian

vortices of initial radius a_i , circulation Γ_i , separated by an initial distance b_i :

$$\omega_i = \frac{\Gamma_i}{\pi a_i^2} \left(\exp \left(-\frac{(x - \frac{b_i}{2})^2 + y^2}{a_i^2} \right) + \exp \left(-\frac{(x + \frac{b_i}{2})^2 + y^2}{a_i^2} \right) \right). \quad (6)$$

This two-dimensional simulation is conducted for the same set of parameters (n_x, n_y, L_x, L_y, ν) as the 3D simulation. Each vortex is deformed by the strain field created by the companion vortex and becomes slightly elliptical [15–18]. Then, the vortex core a increases slowly by diffusion whereas the distance b remains constant. The velocity field \mathbf{U}_{2D} is taken during this quasi-steady phase when the ratio a/b has reached the desired initial value a_0/b_0 for the 3D numerical simulation. The two-dimensional simulation is also continued further in order to have a reference simulation to analyze the 3D simulations. The linear stability analysis of the base flow \mathbf{U}_{2D} is also conducted in order to find the most unstable vertical wavenumber k_{zm} and eigenmode \mathbf{U}' [13]. The eigenmode \mathbf{U}' is normalized so that its total energy per unit vertical length scale is equal to unity.

Space and time are non-dimensionalized respectively by the core size a_0 and by the inverse of the vorticity at the center of each vortex $\tau = \pi a_0^2 / \Gamma_0$, where Γ_0 is the circulation of each individual vortex at time t_0 . The same notation is kept for the non-dimensional variables for the sake of simplicity. The Reynolds number is defined as $Re = \frac{t_0}{\nu}$ and the Froude number is $F_h = \frac{t_0}{\pi a_0^2 N}$. The Schmidt number $Sc = \nu/D$ is set to unity.

3. Qualitative behavior of the pairing of vortices in a stratified flow

The dynamics of the merging of two co-rotating vortices in a linearly stratified flow has been first computed without the sophisticated initial condition described above. The evolution of two gaussian vertical vortices perturbed by a low amplitude 3D white noise has been computed in a cubic box and with a moderate resolution 128^3 . The initial ratio between the core size a_i and separation distance b_i is $a_i/b_i = 0.15$. The initial Froude number is $F_h = 1.33$ and the Reynolds number is $Re = 2120$. The size of the domain is $L_x = L_y = L_z = 10\pi a_i$. Fig. 1 shows the temporal evolution of the vertical vorticity. At the beginning of the simulation ($t = 0$), the vortices are columnar and rotate one around the other at angular velocity $\Omega_i = \Gamma_i / (\pi b_i^2)$. At time $t = 478$, the two vortices are displaced symmetrically alternately closer and away along the vertical in a direction making a well defined angle with the line joining the vortex centers. As a result, the distance between the two vortex axes oscillates along the vertical. This perturbation structure is similar to the one associated with the zigzag instability described by Otheguy et al. [13]. At $t = 557$, the pairing of the vortices has occurred in layers where they were brought closer by the instability. These layers alternate with layers where two well-separated vortices are still rotating one around the other. At $t = 955$, merging has eventually occurred at each vertical station. The final vortex displays a variation of core size along the vertical resulting from the desynchronized pairing. This modulated core is surrounded by low intensity spiral arms (yellow contours).

The vertical wavelength that shows up spontaneously is $\lambda/(bF_h) = 0.5$ with a spatial variability of about 16%, in good agreement with the most unstable wavelength of the zigzag instability $\lambda/(bF_h) = 0.64$ predicted by the linear stability analysis by [13]. Furthermore, the instability manifests itself even at finite amplitude, as bending deformations of the vortices in agreement with

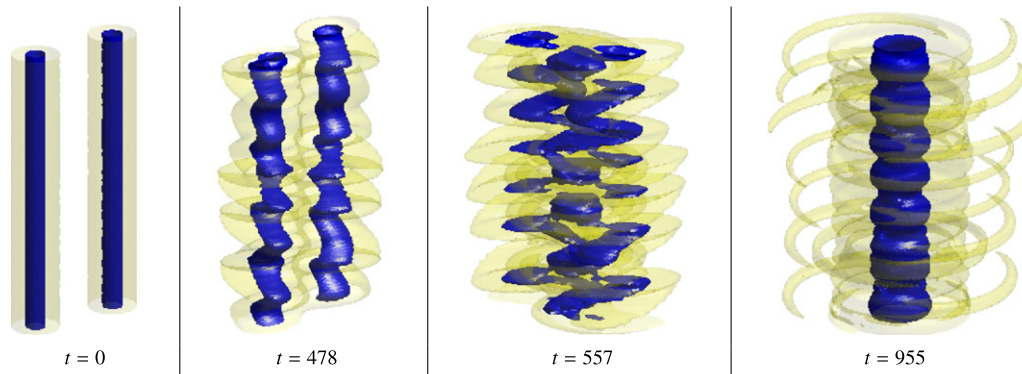


Fig. 1. Vertical vorticity contours obtained by DNS of two co-rotating vertical vortices for $a_i/b_i = 0.15$, $F_h = 1.33$, $Re = 2120$ and a moderate resolution 128^3 . Yellow and blue contours represent respectively 5% and 50% of the instantaneous maximum vorticity. (For interpretation of the references to color in this figure legend, the reader is referred to the web version of this article.)

the linear theory predictions. These two features indicate that the non-linear dynamics of the pairing in a stratified flow, and in particular the associated vertical variations, is controlled by the linear zigzag instability. Therefore, it is legitimate to limit the computational domain to one vertical wavelength and to initialize the perturbation by the leading eigenmode. This procedure will allow to use a very flat box, i.e. to reduce the number of points along the vertical for a given spatial resolution. By this way, one can achieve larger Reynolds numbers than if cubic boxes were used.

4. Description of merging in a strongly stratified fluid

In this section, the typical 3D evolution of the vortex pair is described for a Reynolds number equal to 2000. The horizontal size of the computational domain is $L_x = L_y = 30$, which is large enough to minimize the effects of the periodic boundary conditions. The number of horizontal collocation points is $n_x = n_y = 512$ giving a reasonably fine mesh to resolve the vortex core and the small scales that appear during the evolution. The time step is $\delta t = 0.01$. The ratio between the core size of the vortices a_0 and their separation distance b_0 is initially $a_0/b_0 = 0.15$. The Froude number is $F_h = 1$. The vertical size of the box is adjusted to correspond to the most unstable zigzag instability wavelength: $L_z = 4.2$ implying that $n_z = 72$ since the same resolution is used in the vertical and horizontal directions. The initial perturbation amplitude is $A = 0.001$ corresponding to an initial horizontal vorticity with a value of the vertically averaged maximum ($M_h = 0.007$) more than two orders of magnitude lower than the value of the vertically averaged maximum of the total vorticity ($M_t = 1$).

Fig. 2 displays the temporal evolution of the total (left column), vertical (central column) and horizontal (right column) vorticity fields. The time origin is taken at the beginning of the 3D simulation. The evolution is qualitatively similar to the one of the randomly forced case (Fig. 1).

At $t = 290$, the zigzag instability has displaced symmetrically the two vortices and driven them closer at the top and bottom of the periodic box and farther in the central region of the domain. The horizontal vorticity magnitude has strongly increased ($M_h = 0.481$) and is comparable to the vertical vorticity magnitude ($M_z = 0.488$).

At time $t = 350$ (Fig. 2), the merging has occurred at the top and bottom (layer thereafter called \mathcal{L}_1) where the vortices were brought closer together by the instability whereas they keep being well separated in the central layer (thereafter called $\mathcal{L}_{1/2}$). The four horizontal cross-sections of the vertical vorticity field (distant by a quarter of a wavelength from each other) shown in Fig. 3

confirm that in layer $\mathcal{L}_{1/2}$ (section $\mathcal{S}_{1/2}$ located at $z = 1.8^1$), the two vortices are separated whereas they have merged in the three other cross-sections. Fig. 2 at $t = 350$ displays a complex entanglement of thin horizontal structures of horizontal vorticity with a magnitude ($M_h = 0.404$) larger than the vertical vorticity maximum ($M_z = 0.324$).

At time $t = 480$, vertical vorticity contours show that the pairing is not yet completed in the central layer $\mathcal{L}_{1/2}$. The horizontal vorticity field exhibits on each side of the layer $\mathcal{L}_{1/2}$ four spiraling arms with a magnitude ($M_h = 0.139$) three times smaller than at time $t = 350$.

At $t = 750$, the merging has occurred in all the layers and the final vortex displays variations in the core size along the vertical direction (Fig. 2). The horizontal vorticity is small ($M_h = 0.045$, to be compared to $M_z = 0.206$) but still exhibits two separated blobs.

In summary, the zigzag instability makes the merging non-simultaneous along the vertical and creates strong horizontal vorticity between layers before the merging is completed.

5. Analysis of a 3D stratified pairing and comparison with a 2D pairing

5.1. Evolution of the separation distance and of the core size of the vortices

The time-evolution of the vortex pair is analyzed by fitting the vertical vorticity $\omega_z(x, y, z, t)$ in horizontal cross-sections at each vertical position by two gaussian vortices separated by a distance $b(z, t)$, with an instantaneous circulation $\Gamma(z, t)$ and a core size $a(z, t)$. This fit of the vertical vorticity is more than 5% accurate except just when the vortices are merging in the layer considered showing that during their evolution the vortices keep being gaussian.

The same fit is first performed for the 2D simulation and the results are plotted in Fig. 4 as a plain line. We observe that the evolution of vortices before merging exhibits several distinct phases as previously described for example in [19–22]. Since, the vortices are initially adapted to the strain field generated by the companion vortex, the first phase here consists in the viscous phase: the separation distance between the vortices b (Fig. 4b) remains almost constant while the vortex core size a (Fig. 4a) evolves slowly by viscous diffusion. The total duration of this phase scales like Re^2 . The second phase is fast and corresponds

¹ Note that the maximum of the bending deformations due to the zigzag instability is not located at the center of the box $z = 2.1$ but at $z = 1.8$.

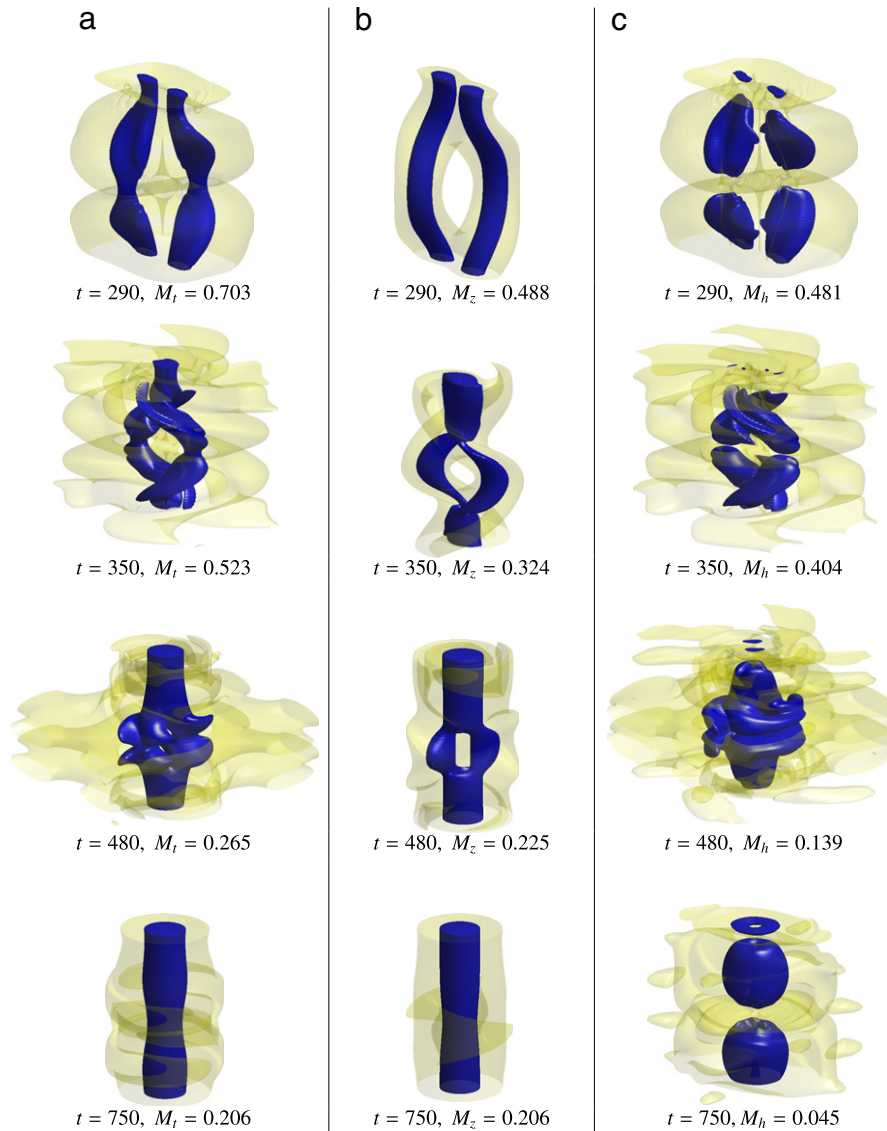


Fig. 2. (a) Total, (b) vertical, (c) horizontal vorticity isosurfaces yellow and blue surfaces represent respectively 5% and 50% of the magnitude of the field considered (M_t , M_z , M_h) defined as the vertically averaged maximum in each horizontal cross-section obtained by DNS of two co-rotating vertical vortices for $a_0/b_0 = 0.15$, $F_h = 1$, $Re = 2000$ and $A = 0.001$. (For interpretation of the references to color in this figure legend, the reader is referred to the web version of this article.)

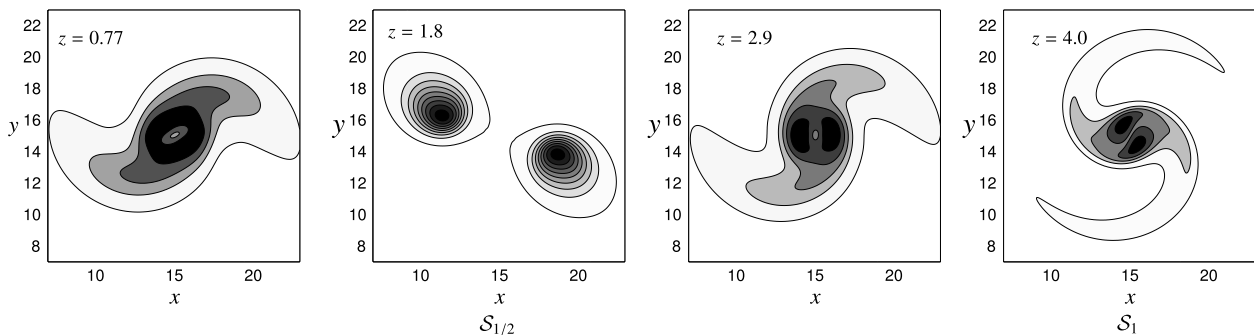


Fig. 3. Horizontal cross-sections of the vertical vorticity field (plotted in Fig. 2b) at time $t = 350$ and at four different vertical locations separated by a quarter of a wavelength: at $z = 0.77$, $z = 1.8$ (section $S_{1/2}$), $z = 2.9$, $z = 4.0$ (section S_1) for $a_0/b_0 = 0.15$, $F_h = 1$, $Re = 2000$ and $A = 0.001$.

to a convective process where the separation distance between the vortices drops rapidly as they merge. Meunier et al. [21] have shown that this convective merging is initiated when the ratio a/b reaches the critical value $(a/b)_c \sim 0.29$. Cerretelli and Williamson [22] identified a third phase (the beginning of which is

barely visible in Fig. 4b) where two vorticity maxima are present inside the merged vortex at a distance oscillating around $0.28 b_0$ (indicated by a dotted line in Fig. 4b). These two maxima inside the vortex core eventually disappear being smoothed out by viscous diffusion.

Results from the three-dimensional stratified simulation for the same Reynolds number as the 2D simulation are also reported in Fig. 4 for the two horizontal cross-sections $\delta_{1/2}$ ($z = 1.8$) and δ_1 ($z = 4$) (respectively the center of the layers $\mathcal{L}_{1/2}$ and \mathcal{L}_1). We consider that the vortices have merged when their separation distance falls below the value $b_c = 0.28b_0$ indicated by a dotted line in Fig. 4(b). We observe that in both cross-sections $\delta_{1/2}$ and δ_1 , the merging occurs earlier than in the two-dimensional case but is not simultaneous as already observed in Figs. 1–3. In a first stage, the separation distances $b_{1/2}$ and b_1 between the two vortices in the cross-sections $\delta_{1/2}$ and δ_1 respectively decrease and increase exponentially as predicted by the linear stability analysis:

$$b_{1/2}(t) = b_0 + A_b A \exp(\sigma t) \quad (7)$$

$$b_1(t) = b_0 - A_b A \exp(\sigma t), \quad (8)$$

where A is the initial amplitude of the perturbation given in the caption, σ the non-dimensional growth rate of the zigzag instability ($\sigma \approx a_0^2/b^2 \approx 0.02$) and $A_b \approx 6.5$ is a theoretical constant predicted with no fitting parameter giving the displacement in the direction of the line joining the vortex centers for the normalized eigenmode \mathbf{U}' .

The theoretical predictions (7) and (8), plotted as dashed lines in Fig. 4(b), match remarkably well the observations. For b_1 , the exponential decay keeps being valid until the vortices merge in δ_1 at time $t_1 \approx 365$ suggesting that the pairing in δ_1 is not driven by a convective merging process as in the 2D case but by the linear zigzag instability (Fig. 4b). In the section $\delta_{1/2}$, the distance $b_{1/2}$ starts increasing exponentially as predicted by (7) before slowing down after the merging being completed in δ_1 , and then rapidly decreases leading to an anticipated merging at $t_{1/2} \approx 590$.

The core size of the vortices a initially follows the two-dimensional viscous evolution according to the diffusion law [23]:

$$a(t) = \sqrt{a_0^2 + 4vt}, \quad (9)$$

plotted as dashed line in Fig. 4(a). After this initial stage, the core size a increases rapidly in section δ_1 (Fig. 4a) while the pairing occurs (from $t \approx 300$ to $t \approx 400$) and then increases slowly following nearly a viscous diffusion law as indicated by the dashed line in Fig. 4(a). The core size in $\delta_{1/2}$ also starts increasing at the same time as in δ_1 but keeps increasing till the pairing is completed in $\delta_{1/2}$ ($t_{1/2} \approx 590$). By approximating and extrapolating the vortex cores evolution before and after the merging by the diffusion law (9), we estimate an increase of the core size by a factor 1.4 in section δ_1 and by a factor 2 in $\delta_{1/2}$ (Fig. 4b) at the time when the vortices have just merged.

Fig. 5 shows the evolution of the vortex core size $a(z, t)$ (Fig. 5a) and of the separation distance $b(z, t)$ between the vortices rescaled by b_0 (Fig. 5b) as a function of time and of the vertical location. Data of Fig. 4 correspond to the cross-sections $\delta_{1/2}$ at $z = 1.8$ and δ_1 at $z = 4$ of these surfaces. The distance b/b_0 falls below the value 0.3 at time $t_1 \approx 365$ (Fig. 5b) simultaneously in the whole layer \mathcal{L}_1 (from $z = 0$ to $z = 1$ and from $z = 2.6$ to $z = 4.2$) meaning that the pairing is synchronized in the whole layer \mathcal{L}_1 . The pairing also occurs almost simultaneously around $t_{1/2} \approx 590$ in layer $\mathcal{L}_{1/2}$ i.e. between $z = 1$ and $z = 2.6$. Sharp vertical gradients are formed on the frontier between $\mathcal{L}_{1/2}$ and \mathcal{L}_1 . The evolution of the vortex core size (Fig. 5a) is more complex. A slow viscous diffusion is followed by extremely fast evolutions at the frontier between \mathcal{L}_1 and $\mathcal{L}_{1/2}$ (around $t_1 = 365$) where the vertical shear due to the decorrelation induced by the zigzag instability is maximum. Subsequently, a fast evolution occurs in the middle of the layer $\mathcal{L}_{1/2}$ just before the pairing event ($t_{1/2} = 590$).

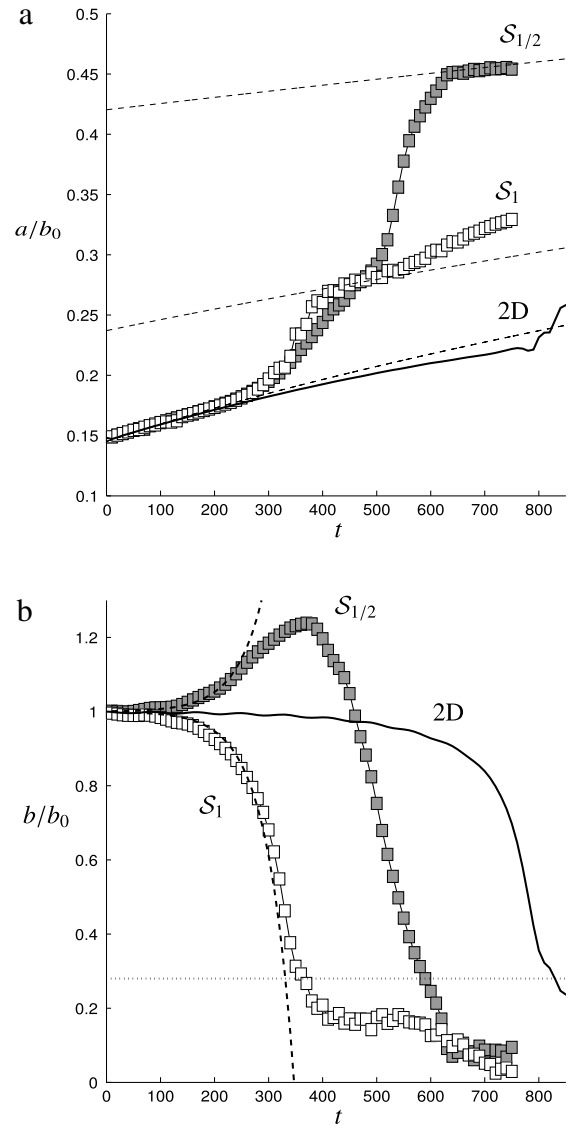


Fig. 4. Evolution of (a) the vortex cores size a non-dimensionalized by b_0 , (b) the separation distance between the vortex centers b non-dimensionalized by b_0 , for $a_0/b_0 = 0.15$, $F_h = 1$, $Re = 2000$, $A = 0.001$. The solid lines represent the 2D case and the symbols the 3D stratified case, open symbols being measured in section δ_1 and closed symbols in section $\delta_{1/2}$ i.e. (a) $a_1 = a(z = 4, t)$, $a_{1/2} = a(z = 1.8, t)$ and (b) $b_1 = b(z = 4, t)$, $b_{1/2} = b(z = 1.8, t)$. The viscous diffusion law (Eq. (9)) is represented by dashed lines in (a) to fit the evolution of the initial and merged vortices. In (b), the predictions of the linear theory of the zigzag instability (Eqs. (7)–(8)) are represented by dashed lines and the merging criterion $b_c = 0.28b_0$ is plotted by a dotted line giving $t_1 \approx 365$ and $t_{1/2} \approx 590$ for the time of merging in sections δ_1 and $\delta_{1/2}$.

5.2. Effect of the parameters: amplitude perturbation, Reynolds number Re and Froude number F_h

Fig. 6(a) investigates the effect of the amplitude of the initial perturbation A for $F_h = 0.5$ and $Re = 2000$. The curves representing b are simply time-shifted in both layers so that a higher A corresponds to an earlier merging in section δ_1 as well as in section $\delta_{1/2}$. The time delay $\Delta t = t_1 - t_{1/2}$ between the mergings in the different layers is almost independent of the initial perturbation amplitude A and so does the maximum separation distance between the vortices reached in $\delta_{1/2}$. This confirms that the zigzag instability controls the pairing in a stratified fluid. The instant t_1 of the pairing in δ_1 may be then estimated by the instant when b_1

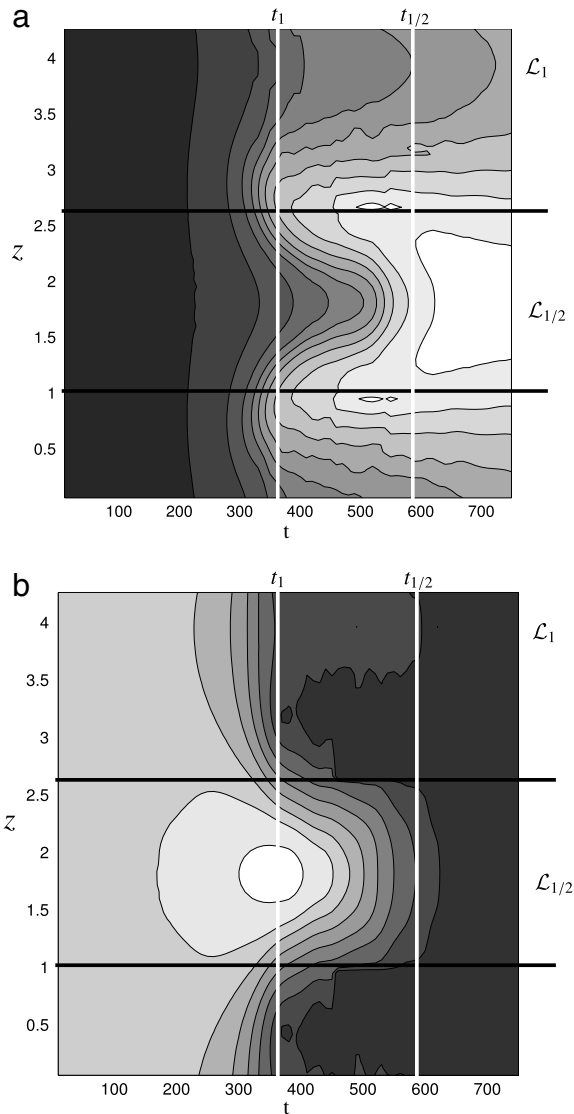


Fig. 5. Contours of (a) vortex core size $a(z, t)$ and (b) separation distance between the vortex centers $b(z, t)$ rescaled by b_0 as a function of time and of vertical location. The contour level is 0.03 in (a) starting at $a/b_0 = 0.15$ at $t = 0$. In (b), the contour level is 0.15 starting at $b/b_0 = 1$ for $t = 0$. The white color represents the larger values. The bold horizontal lines delimit the layers \mathcal{L}_1 and $\mathcal{L}_{1/2}$. The white vertical lines indicate the times of merging in layers \mathcal{L}_1 and $\mathcal{L}_{1/2}$.

given by (8) vanishes:

$$t_1 \approx \frac{1}{\sigma} \ln \left(\frac{b_0}{A_b A} \right). \quad (10)$$

This equation predicts that the time delay $t_1(A = 0.001) - t_1(A = 0.005) = \ln 5/\sigma \approx 100$ which is well verified in Fig. 6(a). Fig. 6(b) shows the effect of the Reynolds number on the stratified merging. When the Reynolds number increases, the time t_1 of the merging in section \mathcal{L}_1 decreases whereas in the two-dimensional case (plotted in full line for $Re = 2000$ and in dashed line for $Re = 5000$), the time to merge increases dramatically with Re from $t \approx 800$ to $t \approx 1700$ (not visible in the figure). For $Re = 8000$, the 2D pairing would occur for an even larger time. The acceleration of the merging with Re in \mathcal{L}_1 is

$$\frac{t_1(Re = 5000)}{t_1(Re = 2000)} \approx 0.80 \quad (11)$$

and is due to the increase in the zigzag instability growth rate from $\sigma = 0.016$ at $Re = 2000$ to $\sigma = 0.019$ at $Re = 5000$ [13] since

Eq. (10) predicts:

$$\frac{\sigma(Re = 2000)}{\sigma(Re = 5000)} \approx 0.84. \quad (12)$$

The evolution of b_1 when Re is varied from 5000 to 8000 remains almost similar since the variation of the growth rate is negligible between these Reynolds numbers. The distance between the vortices in the layer $\mathcal{L}_{1/2}$, i.e. $b_{1/2}$, increases initially faster when Re is increased from $Re = 2000$ to $Re = 5000$, again because of the increase of the growth rate. The maximum value of $b_{1/2}$ increases with the Reynolds number but is reached at about the same time for all Re . A rapid decrease then follows when the pairing in $\mathcal{L}_{1/2}$ begins. Because $\max(b_{1/2})$ increases with Re , the time $t_{1/2}$ increases also slightly with the Reynolds number. The delay $\Delta t = t_{1/2} - t_1$ in the pairing between \mathcal{L}_1 and $\mathcal{L}_{1/2}$ increases with Re from $\Delta t = 85$ for $Re = 2000$ to $\Delta t = 215$ for $Re = 5000$ and $\Delta t = 270$ for $Re = 8000$.

Fig. 6(c) is similar to Fig. 6(b) but for $F_h = 1$. In that case, the evolution of b_1 is almost independent of the Reynolds number in agreement with the fact that for $F_h = 1$ the difference between the growth rates of the instability for $Re = 2000$ ($\sigma = 0.01995$) and $Re = 5000$ ($\sigma = 0.0206$) is much smaller than for $F_h = 0.5$. In contrast, the maximum value of the distance $b_{1/2}$ strongly increases with the Reynolds number and reaches $1.6b_0$ for $Re = 10000$. The delay $\Delta t = t_{1/2} - t_1$ between the mergings in \mathcal{L}_1 and $\mathcal{L}_{1/2}$ again increases from $\Delta t = 225$ at $Re = 2000$ to $\Delta t = 400$ at $Re = 5000$ and $\Delta t = 500$ at $Re = 10000$.

This strong dependence of the merging delay Δt on Re evidenced both for $F_h = 0.5$ (Fig. 6b) and $F_h = 1$ (Fig. 6c) suggests that the merging in $\mathcal{L}_{1/2}$ is viscously driven by the merging in \mathcal{L}_1 . But the viscous time scale $t_v = L_z^2/4\nu$ – built on $L_z/2$ – is 26 to 100 times larger than Δt suggesting that the pairing in $\mathcal{L}_{1/2}$ involves an interaction between viscous and inertial or buoyancy effects. Indeed, in the next section, it will be shown that a very large vertical shear whose intensity depends on the Reynolds number appears between the two layers. Thus, the estimation of t_v should be based on the vertical scale characterizing this shear. Furthermore, it is noticeable that once the decrease of $b_{1/2}$ is initiated, the slope of this decrease is independent of the Reynolds number.

Fig. 6(d) investigates the effect of the Froude number on the time evolution of the separation distances b_1 and $b_{1/2}$. We observe that t_1 increases when the Froude number decreases. This is due to the increase of the growth rate of the zigzag instability with the Froude number (for $Re = 2000$, $\sigma = 0.02$ for $F_h = 1$, $\sigma = 0.016$ for $F_h = 0.5$ and $\sigma = 0.011$ for $F_h = 0.3$) owing to the vertical viscous dissipation. The latter indeed decreases as the Froude number increases because the most unstable wavelength of the zigzag instability scales like F_h [13].

To summarize, when the flow is strongly stratified, the merging of two co-rotating vortices is induced by the growth of the zigzag instability. In the layer \mathcal{L}_1 where the zigzag instability pushes together the vortices, the merging time t_1 is well predicted by the exponential growth of the instability and thus depends on F_h and Re only through the instability growth rate. The dynamics in the layer $\mathcal{L}_{1/2}$ is more complex since the vortices start moving away exponentially due to the zigzag instability but once the pairing is completed in \mathcal{L}_1 , the resulting vertical inhomogeneity of the flow seems to force the pairing in that layer. The time delay Δt between the pairings in \mathcal{L}_1 and $\mathcal{L}_{1/2}$ is a function of both F_h and Re but its moderate increase between $Re = 5000$ and $Re = 10000$ suggests that it is not a simple diffusion process that drives the vertical correlation.

Like Fig. 5b, Fig. 7 presents the evolution of the horizontal distance b between the vortex cores as a function of z and t for a Froude number $F_h = 1$ and two Reynolds numbers $Re = 5000$ and $Re = 10000$. In the two cases, the pairing is synchronized in layer \mathcal{L}_1 and in the center of layer $\mathcal{L}_{1/2}$. The size of the synchronized area in $\mathcal{L}_{1/2}$ decreases with Re and the vertical variations of b are confined to thin layers whose thickness decreases with Re .

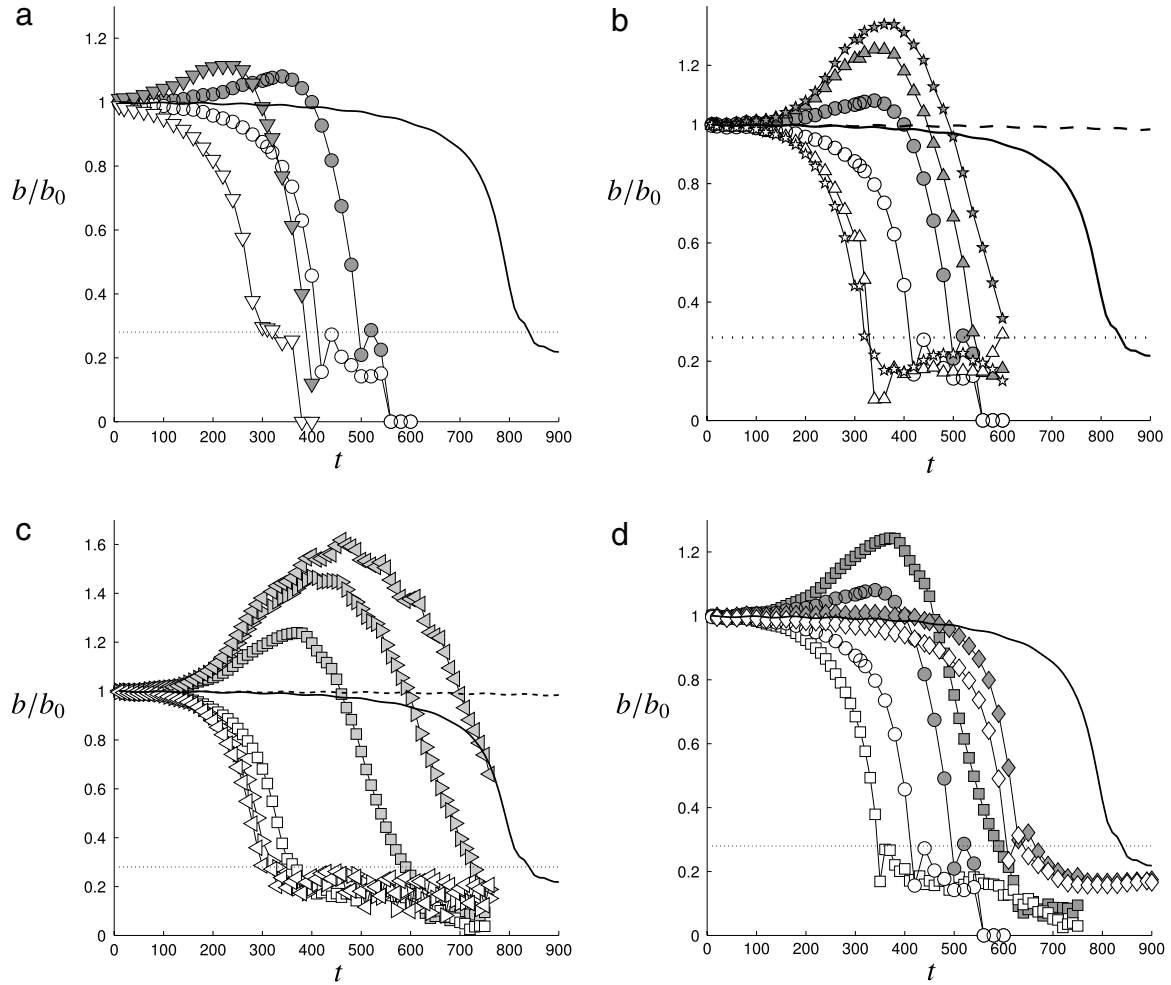


Fig. 6. Evolution of the separation distances b_1 and $b_{1/2}$ between the vortex centers for $a_0/b_0 = 0.15$; same as Fig. 4(b) but (a) for different perturbation amplitude (\circ) $A = 0.001$; (∇) $A = 0.005$ with $F_h = 0.5$, $Re = 2000$; (b) for different Reynolds numbers (\circ) $Re = 2000$; (Δ) $Re = 5000$; (\star) $Re = 8000$ with $A = 0.001$, $F_h = 0.5$; (c) for different Reynolds numbers (\square) $Re = 2000$; (\triangleright) $Re = 5000$; (\triangleleft) $Re = 10\,000$ with $A = 0.001$, $F_h = 1$; (d) for different Froude numbers (\square) $F_h = 1$; (\circ) $F_h = 0.5$; (\diamond) $F_h = 0.3$ with $A = 0.001$, $Re = 2000$. The solid and dashed lines represent the two-dimensional simulations corresponding to $Re = 2000$ and $Re = 5000$, respectively.

6. Energy and enstrophy analysis

6.1. Dissipation and small scale generation

To further analyze the dynamics of the pairing, we computed the mean total kinetic energy $E_K = 1/(2n_x n_y n_z) \sum_{x,y,z} |\mathbf{u}|^2$ and the mean total enstrophy $Z = 1/(2n_x n_y n_z) \sum_{x,y,z} |\boldsymbol{\omega}|^2$ (Fig. 8). These quantities have been also decomposed into vertical and horizontal components. The potential energy $E_p = F_h^2/(2n_x n_y n_z) \sum_{x,y,z} \rho^2$ has been also computed but its maximum is very low compared to the maximum of the kinetic energy. The vertical velocity contribution to the total kinetic energy is negligible (it appears as a continuous line on the x -axis in Fig. 8a). The evolution of the total kinetic energy can be divided into three phases. During the first phase (from $t = 0$ to $t = 250$), the total kinetic energy slowly decreases as in the 2D (case plotted as a thin plain line). Around $t = 250$, i.e. when the zigzag instability has reached a finite amplitude, the kinetic energy decreases quickly till the pairing is completed in \mathcal{L}_1 ($t_1 \approx 365$). The loss of kinetic energy is about 20% compared to the 2D case. During the third phase (from $t = 250$ to $t = 750$), the kinetic energy decreases at a slightly slower rate than in the 2D simulation.

The vertical enstrophy (Fig. 8b) follows the same trend as the kinetic energy: the vertical enstrophy of the 3D simulation departs from the enstrophy of the 2D simulation around $t = 250$,

decreases by about 50% when reaching the time when the pairing is completed in \mathcal{L}_1 and then decreases slightly slower than in the 2D simulation. The horizontal enstrophy (Fig. 8b) is approximately zero at the beginning and at the end of the simulation. In between, it bursts out and reaches twice the initial value of the total enstrophy around $t_1 = 365$, i.e. at the time where the vortices in layer \mathcal{L}_1 are just merging. This generation of horizontal vorticity comes from the vertical shear generated by the shifted positions of the vortices between layers $\mathcal{L}_{1/2}$ and \mathcal{L}_1 . Then it decreases rapidly and vanishes after $t_{1/2} = 590$ when the positions of the vortex centers are nearly aligned along the vertical direction.

Figs. 9(a) and 10(a) investigate the effect of the amplitude A of the initial perturbation and show that the energy loss and the enstrophy production are nearly independent of the value of A but occur sooner when the amplitude is larger. The enstrophy production is slightly smaller when the initial amplitude is smaller because the pairing occurs later so that the vortices have been more dissipated by horizontal viscous diffusion.

Fig. 9(b–c) investigate the effect of the Reynolds number for Froude numbers $F_h = 0.5$ and $F_h = 1$. We observe that the energy loss compared to the two-dimensional simulations is almost the same for $Re = 5000$ and $Re = 2000$ and seems therefore independent of the Reynolds number.

In contrast, the enstrophy maximum (Fig. 10b) is increased approximately three times for $F_h = 0.5$ when increasing the Reynolds

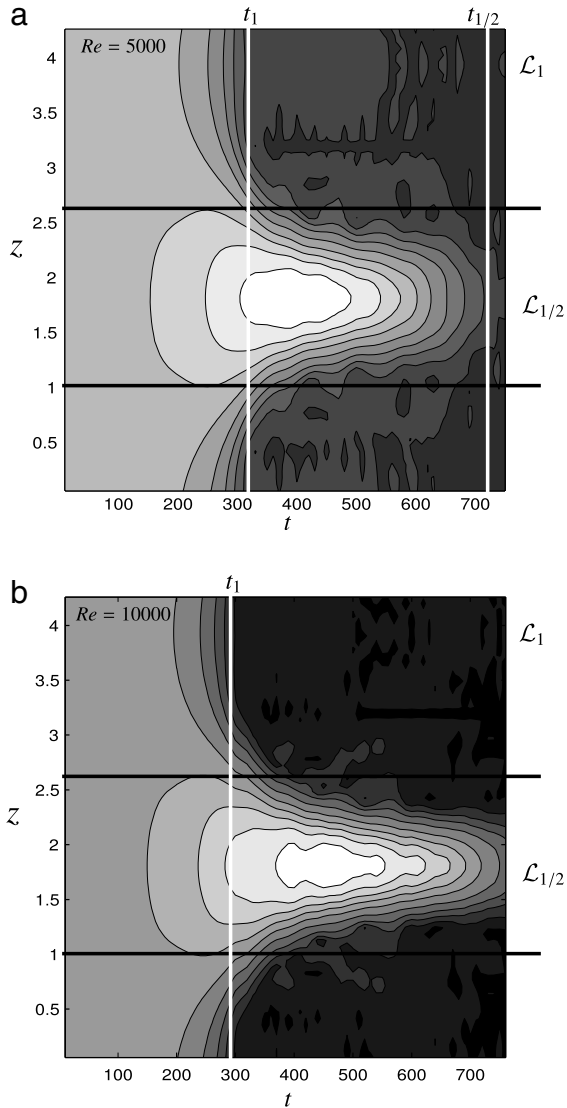


Fig. 7. Same as Fig. 5(b), evolution of the distance between the vortices b (a) for $Re = 5000$ and (b) for $Re = 10000$.

number from $Re = 2000$ to $Re = 5000$ and is multiplied by 4 when increasing the Reynolds number from $Re = 2000$ to $Re = 8000$. Similarly, the enstrophy maximum (Fig. 10c) is multiplied by two for $F_h = 1$ when increasing the Reynolds number from $Re = 2000$ to $Re = 5000$ and is multiplied by 2.5 when increasing the Reynolds number from $Re = 2000$ to $Re = 10000$. Comparing Fig. 10(b) and 10(c), the enstrophy maximum for $Re = 5000$ is two times larger for $F_h = 0.5$ than for $F_h = 1$ whereas from Fig. 9(b) and 9(c), the energy loss is only 25% larger for $F_h = 0.5$.

Fig. 9(d) shows the evolution of the total kinetic energy for $Re = 2000$ and different Froude numbers. The curves corresponding to $F_h = 1$ and $F_h = 0.5$ nearly superimpose whereas the curve corresponding to $F_h = 0.3$ exhibits a much smaller decrease in energy. The corresponding evolution of total enstrophy is shown in Fig. 10(d). We observe that the enstrophy evolution is almost the same for $F_h = 0.5$ and $F_h = 1$. The curve corresponding to $F_h = 0.3$ is much closer to the curves corresponding to the two-dimensional simulation because in this case the growth rate is much lower ($\sigma = 0.011$) and saturation of the perturbation occurs later when about 50% of the energy has already been dissipated.

In summary, when the growth rate of the zigzag instability is close to its inviscid value, the enstrophy production is independent of the Froude number and increases with the

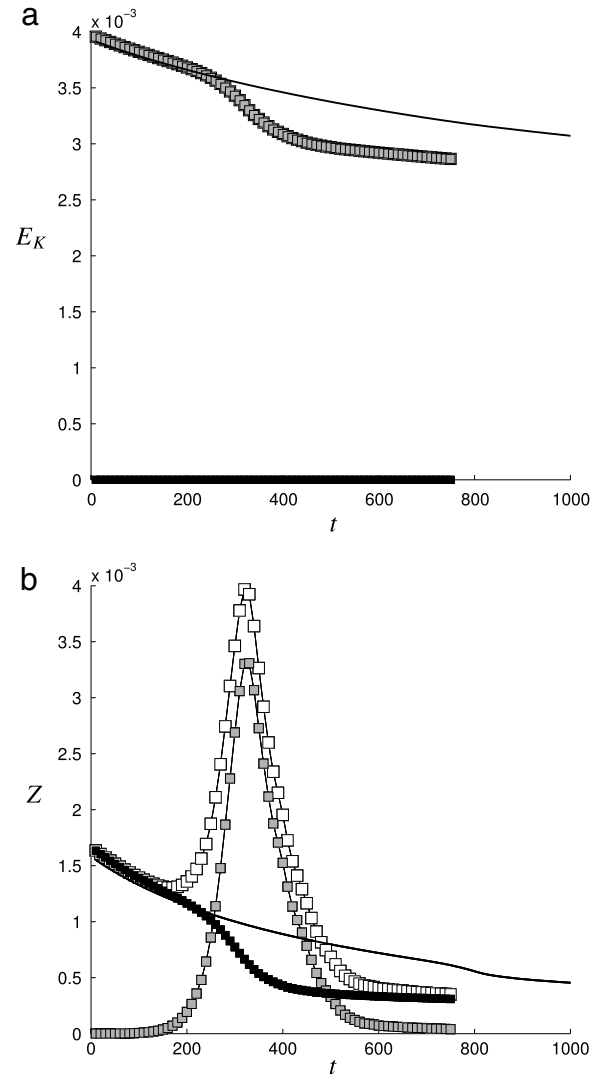


Fig. 8. (a) Mean total kinetic energy $E_K(t)$ and (b) mean total enstrophy $Z(t)$ as a function of time for $a_0/b_0 = 0.15$, $F_h = 1$, $Re = 2000$ and $A = 0.001$ (open symbols). The horizontal and vertical parts of the kinetic energy E_K and of the enstrophy Z are represented by gray and black symbols, respectively. The kinetic energy and enstrophy of the two-dimensional simulation, corresponding to the same set of parameters is plotted by a solid line.

Reynolds number. Fig. 11 shows that the horizontal enstrophy divided by the Reynolds number is approximately independent of the Reynolds and Froude numbers and occurs at a time determined by the initial amplitude of the perturbation. In other words, the maximum enstrophy is approximately inversely proportional to the viscosity like for counter-rotating vortex pairs [24]. If the enstrophy is dominated by the vertical gradients of the horizontal velocity, i.e. $Z \propto |\partial \mathbf{u} / \partial z|^2$, the vertical shear $\partial \mathbf{u} / \partial z$ increases until the associated vertical length scale δ has reached the dissipative scale, i.e. $\delta \propto a / \sqrt{Re}$. This small vertical scale δ will be clearly evidenced in the next section but it is already visible on the enstrophy field (Fig. 2) at the interface between the layers $\mathcal{L}_{1/2}$ and \mathcal{L}_1 .

6.2. Space and time evolutions

We consider the numerical simulation described in Section 5 defined by the set of parameters ($a_0/b_0 = 0.15$, $F_h = 1$, $Re = 2000$, $A = 0.001$). Fig. 12(a–b) shows the evolution of the mean total kinetic energy $\mathcal{E}_K(z, t)$ and mean total enstrophy $\mathcal{Z}(z, t)$ calculated

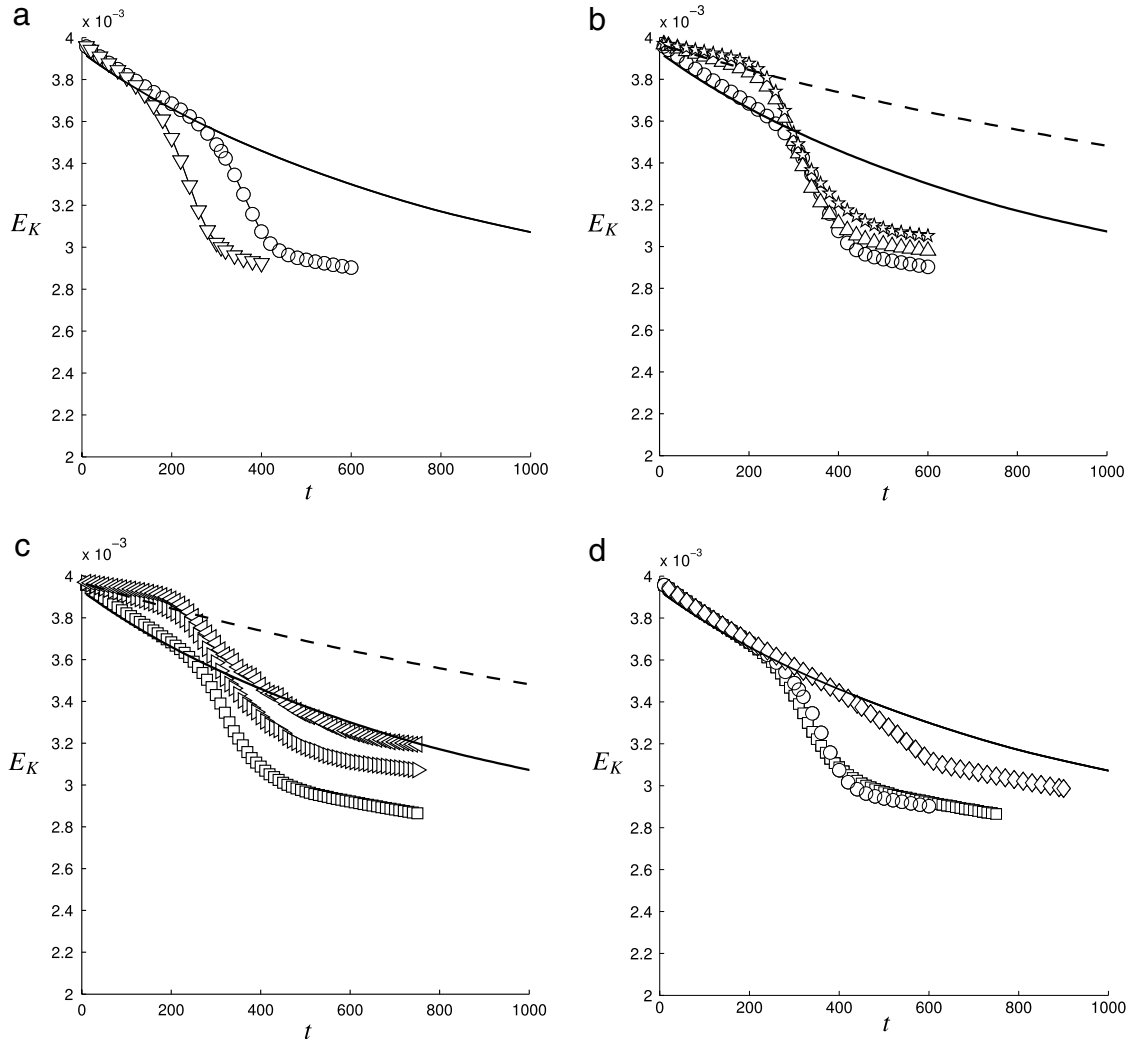


Fig. 9. Evolution of the kinetic energy E_K as a function of time for $a_0/b_0 = 0.15$ and for (a) for different perturbation amplitude (\circ) $A = 0.001$; (∇) $A = 0.005$ with $F_h = 0.5$, $Re = 2000$; (b) for different Reynolds numbers (\circ) $Re = 2000$; (\triangle) $Re = 5000$; (\star) $Re = 8000$ with $A = 0.001$, $F_h = 0.5$; (c) for different Reynolds numbers (\square) $Re = 2000$; (\triangleright) $Re = 5000$; (\triangleleft) $Re = 10\,000$ with $A = 0.001$, $F_h = 1$; (d) for different levels of stratification (\square) $F_h = 1$; (\circ) $F_h = 0.5$; (\diamond) $F_h = 0.3$ with $A = 0.001$, $Re = 2000$. The solid and dashed lines represent the two-dimensional simulations corresponding to $Re = 2000$ and $Re = 5000$, respectively.

in each horizontal layer as a function of time and of the vertical coordinate as

$$\varepsilon_K(z, t) = \frac{1}{2n_x n_y} \sum_{x,y} |\mathbf{u}|^2(x, y, z, t), \quad (13)$$

$$\mathcal{Z}(z, t) = \frac{1}{2n_x n_y} \sum_{x,y} |\boldsymbol{\omega}|^2(x, y, z, t), \quad (14)$$

respectively. From $t = 0$ to $t = 150$, the kinetic energy (Fig. 12a) remains approximately homogeneous along the vertical and is steadily dissipated by viscosity as in 2D. After $t = 150$, the kinetic energy increases in the layer \mathcal{L}_1 and decreases in layer $\mathcal{L}_{1/2}$. This energy transfer is due to the development of the zigzag instability. The energy starts decreasing in layer \mathcal{L}_1 once the pairing is completed in this layer (after $t_1 \approx 365$) and up to the end of the computation. The kinetic energy in $\mathcal{L}_{1/2}$ decreases rapidly till $t = t_1 + \Delta t/2$ and then re-increases slightly when the pairing occurs in $\mathcal{L}_{1/2}$. After the pairing is completed in layer $\mathcal{L}_{1/2}$, it seems that the kinetic energy remains constant in the intermediate layers between \mathcal{L}_1 and $\mathcal{L}_{1/2}$. This suggests that the shear that develops at the frontier between \mathcal{L}_1 and $\mathcal{L}_{1/2}$ is transferring kinetic energy from \mathcal{L}_1 to $\mathcal{L}_{1/2}$. This transfer of kinetic energy might explain that

the pairing in \mathcal{L}_1 seems to drive the pairing in $\mathcal{L}_{1/2}$ in agreement with the observations of the separation distance between the vortices in Section 5.2.

Fig. 12(d) shows that the enstrophy starts with a sinusoidal variation along the vertical when the zigzag instability develops. Then, it concentrates and becomes maximum at the frontier between \mathcal{L}_1 and $\mathcal{L}_{1/2}$ when the merging occurs in layer \mathcal{L}_1 (around $t = t_1$). Enstrophy starts decreasing after the pairing is completed in \mathcal{L}_1 ($t_1 \approx 365$) and is returned to its original value everywhere after $t = 450$.

Fig. 12(b–c) and 12(e–f) are similar to Fig. 12(a) and 12(d), respectively, but for higher Reynolds numbers ($Re = 5000$ for (b) and (e), $Re = 10\,000$ for (c) and (f)). The beginning of the evolutions of the energy and enstrophy are similar for the three Reynolds numbers since it is due to the linear development of the zigzag instability. Then, we see that the evolution occurs on a longer time scale when the Reynolds number is larger. The enstrophy reaches larger values and is concentrated in thinner horizontal layers when the Reynolds number is increased in agreement with the estimate of δ discussed above. These thin layers with intense vertical shear of horizontal velocity move slowly towards the center of the layer $\mathcal{L}_{1/2}$ leading eventually to the pairing in that layer.

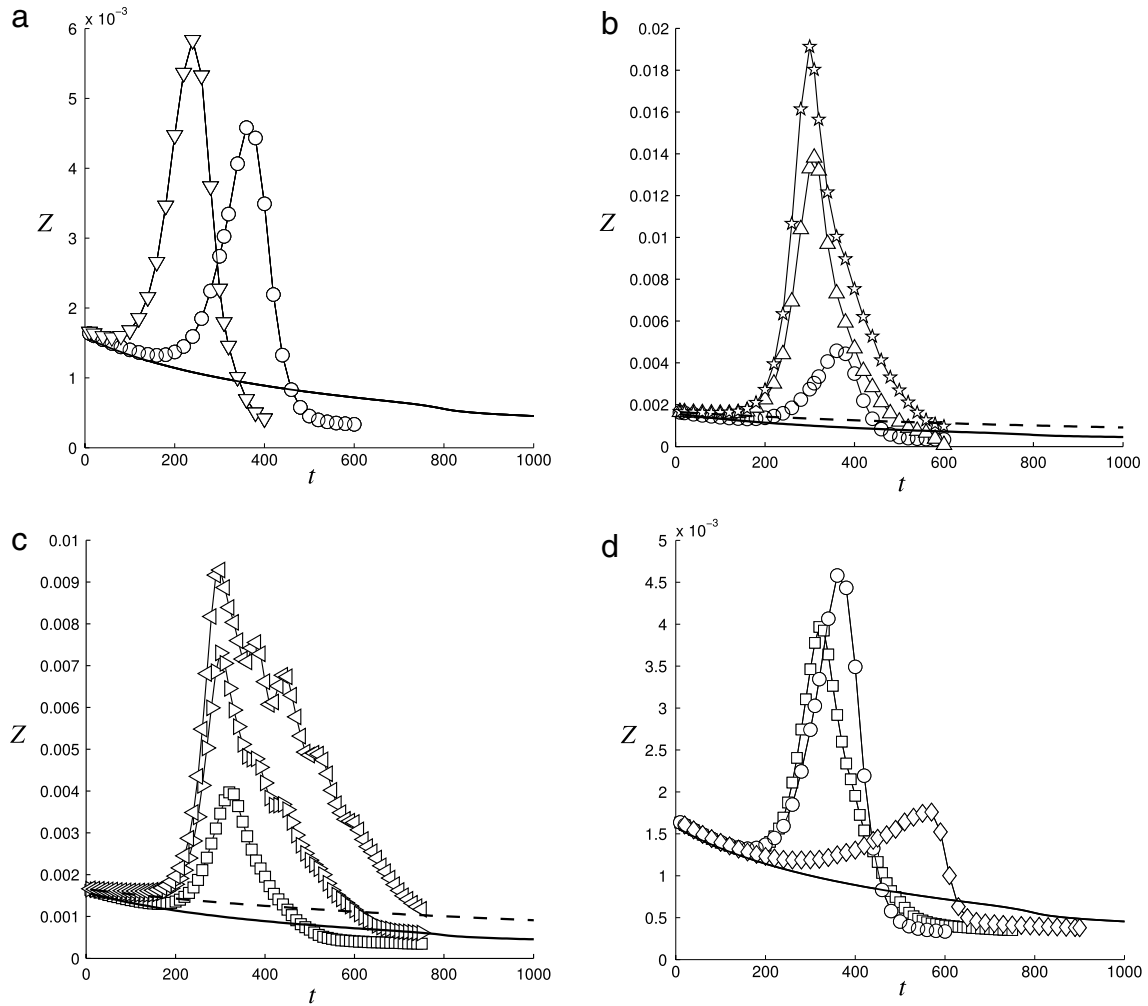


Fig. 10. Same as Fig. 9 except that the enstrophy Z is plotted instead of the kinetic energy.

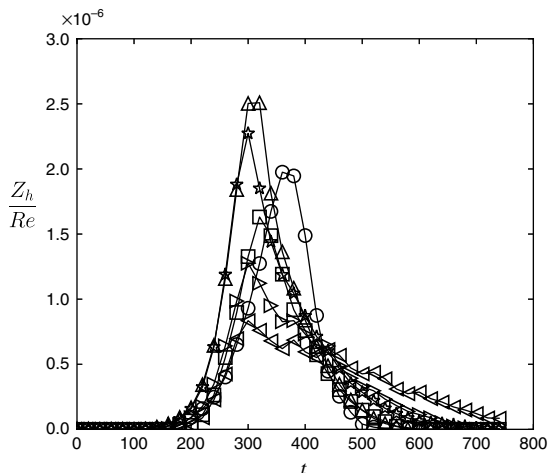


Fig. 11. Time evolution of the horizontal part of the total enstrophy divided by the Reynolds number for $a_0/b_0 = 0.15$, $A = 0.001$ and for (\circ) $Re = 2000$, $F_h = 0.5$; (Δ) $Re = 5000$, $F_h = 0.5$; (\star) $Re = 8000$, $F_h = 0.5$; (\square) $Re = 2000$, $F_h = 1$; (\triangleright) $Re = 5000$, $F_h = 1$; (\triangleleft) $Re = 10000$, $F_h = 1$.

6.3. Search for secondary instabilities

The time evolution of the kinetic energy displayed in Fig. 9 shows that the time integrated dissipation remains approximately

constant even when the Reynolds number is increased to high values (see also Fig. 11). This implies that the energy is transferred towards small scales where it can be dissipated. Assuming that the energy is dissipated only by the vertical shear, we can estimate the characteristic vertical length scale of this shear to be of the order of $\delta = a/\sqrt{Re}$. The stratification can stabilize strong vertical variations of the flow as long as their characteristic vertical length scale is larger than the local buoyancy scale $l_b = aF_h$. This means that the vertical shear between the layers $\mathcal{L}_{1/2}$ and \mathcal{L}_1 should be stable only if the buoyancy Reynolds number $\mathcal{R} = (l_b/\delta)^2 = ReF_h^2$ is not too large. In contrast, for large buoyancy Reynolds number some secondary instabilities might develop like for counter-rotating vortex pairs [24–26].

Augier and Billant [26] have shown that for sufficiently high \mathcal{R} , two different secondary instabilities appear almost simultaneously in distinct regions of counter-rotating vortex pairs due to the development of the zigzag instability. This leads to both high shear on which the Kelvin–Helmholtz instability develops [24] and unstably stratified regions where the convective instability develops [25]. With the definitions of the Reynolds and Froude numbers used in the present study, the condition for the onset of the secondary instabilities is $\mathcal{R} > \mathcal{R}_c \simeq 2700$ in the case of a counter-rotating vortex pair with $a/b = 0.4$ [24].

Even if this threshold is a priori only valid for the particular base state used by Deloncle et al. [24], we can try to compare it to the present simulations as a first approximation. Only two simulations correspond to buoyancy Reynolds number above this

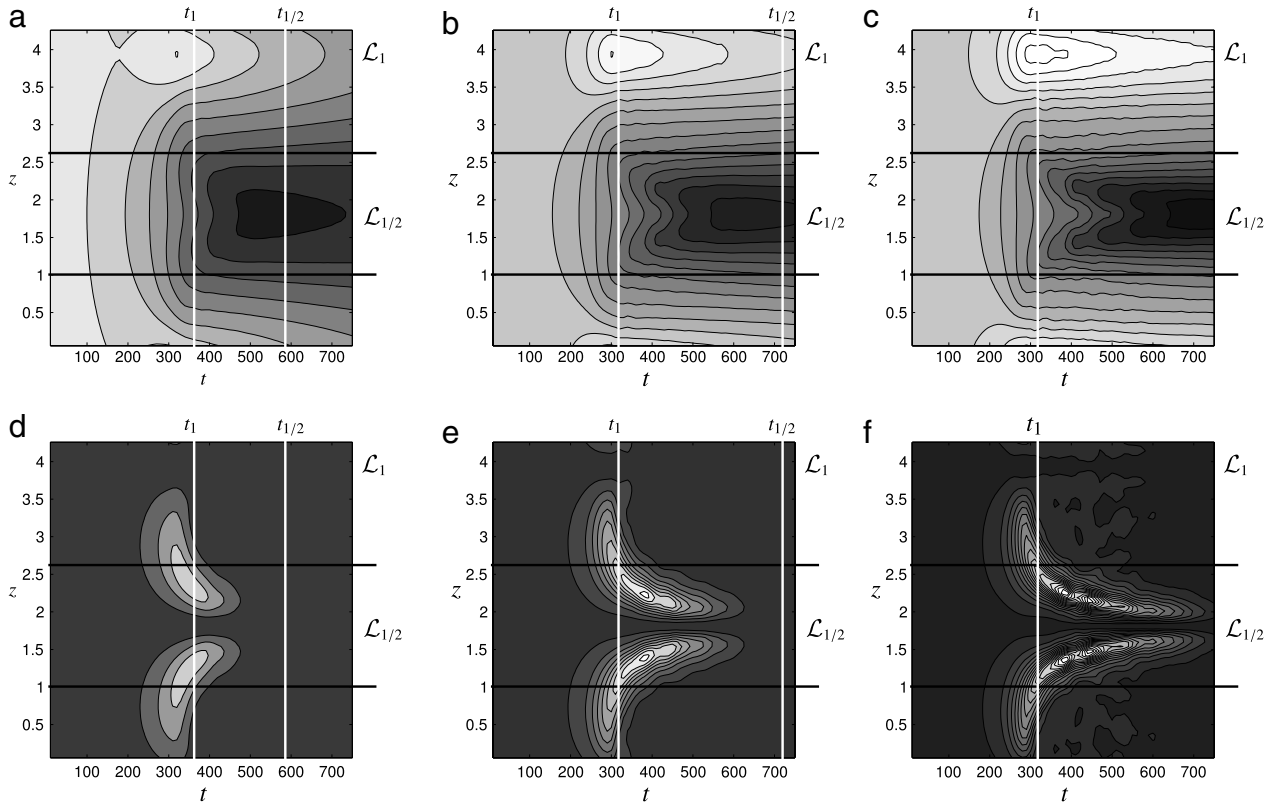


Fig. 12. Kinetic energy $\mathcal{E}_K(z, t)$ (a,b,c) and enstrophy $Z(z, t)$ (d,e,f) as a function of time and vertical location for $a_0/b_0 = 0.15, F_h = 1, A = 0.001$ and (a,d) $Re = 2000$; (b,e) $Re = 5000$; (c,f) $Re = 10\,000$. The contour level of the kinetic energy is 0.0002 and the contour level of the enstrophy is 0.002. White color represents the maximum values.

threshold: $F_h = 1, Re = 5000 \Rightarrow \mathcal{R} = 5000$ and $F_h = 1, Re = 10\,000 \Rightarrow \mathcal{R} = 10\,000$. Indeed, the evolution of the enstrophy in these two simulations (see Figs. 10c and 12e–f) is more irregular and abrupt than in the other simulations which seems to indicate that some particular processes take place for these parameters. However, after a careful study of the flow fields, we have concluded that there is none of the signatures of the secondary instabilities that develop in the case of a counter-rotating vortex pair. In order to investigate further this issue, we have carried out one additional simulation at larger buoyancy Reynolds number ($F_h = 1, Re = 40\,000 \Rightarrow \mathcal{R} = 40\,000$). Such Reynolds number has been achieved without increasing too much the resolution ($n_x = n_y = 512, n_z = 128$) by adding to the Newtonian viscosity a weak hyper-viscosity. This method has been validated against DNS in the case of the transition to turbulence of a dipole in a stratified fluid [27]. Surprisingly, even for this large buoyancy Reynolds number, neither the Kelvin–Helmholtz instability nor the convective instability develops during the pairing.

Fig. 13 shows the color contours of the Richardson number

$$Ri = \frac{-(g/\rho_0)(\partial \rho_{tot}/\partial z)}{|\partial \mathbf{u}_h/\partial z|^2} \quad (15)$$

in a vertical cross-section through the merging vortices. The figure shows also contours of total density (black thin lines). The thick gray lines are iso-lines of vertical vorticity (0.8 times the rms value) indicating the position of the vortices. We see that in the regions between the layers $\mathcal{L}_{1/2}$ and \mathcal{L}_1 where the vertical shear is strong the Richardson number is relatively small but not smaller than 1/4. Interestingly, approximately the same values of the Richardson number are observed for $Re = 10\,000$ which seems to indicate that when the Reynolds number is increased to very high values the Richardson number does not drop to very small values but instead saturates to values close to 1/4. This means that for high buoyancy

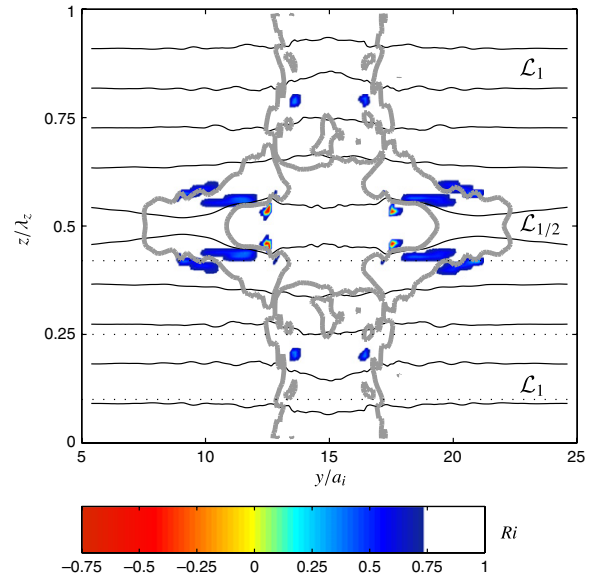


Fig. 13. Snapshot of the Richardson number (colors) and total density (thin black lines) in a vertical cross-section yz during the pairing for $a_0/b_0 = 0.15, F_h = 1$ and $Re = 40\,000$. The thick gray lines are iso-lines of vertical vorticity (0.8 times the rms value) indicating the position of the vortices. The contour interval of total density is approximately equal to 0.4. The three horizontal dotted lines indicate the positions of the horizontal cross-sections in Fig. 14. (For interpretation of the references to color in this figure legend, the reader is referred to the web version of this article.)

Reynolds number the characteristic vertical length scale of the vertical shear scales like the buoyancy length scale l_b and not like the dissipative length scale δ . This scaling law could be explained by the fact that the amplitude of the horizontal displacement of the vortices due to the zigzag instability is geometrically limited to the

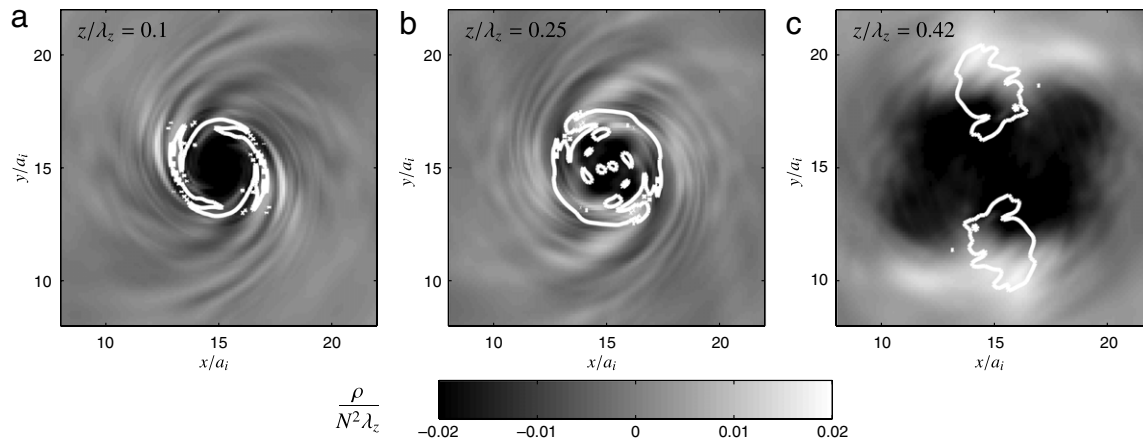


Fig. 14. Snapshot of the normalized density perturbation $\rho/(N^2\lambda_z)$ in three horizontal cross-sections ($z/\lambda_z = 0.1$ in a, 0.25 in b and 0.42 in c as indicated by the horizontal dotted lines in Fig. 13) during the pairing for $a_0/b_0 = 0.15$, $F_h = 1$ and $Re = 40\,000$. The white contours are iso-lines of vertical vorticity (0.8 times the rms value) indicating the position of the vortices.

initial separation distance b_0 in contrast to the case of a counter-rotating vortex pair.

The condition $Ri < 1/4$ somewhere in the flow is a necessary but not sufficient condition for the shear instability of a steady parallel inviscid shear flow [28,29]. However, here the flow is not steady and not parallel which can also affect the threshold for the shear instability. In contrast to the case of a counter-rotating vortex pair the total stratification is stable ($Ri > 0$) except in very small regions explaining why the convective instability does not develop.

Even though the Kelvin–Helmholtz and the convective instabilities do not develop, we see some small scales structures especially in the layer \mathcal{L}_1 . The horizontal energy spectrum is quite shallow, with a slope close to $-5/3$ (not shown), which is consistent with the fact that the dissipation does not decrease to zero even for very large Reynolds numbers. Horizontal cross-sections of the density perturbation field (Fig. 14a) in the layer \mathcal{L}_1 and above (Fig. 14b) show multiple spirals as alternation of white and black shades away from the center of the vortex which could be the signature of waves produced in the regions of strong shear and propagated away and stretched by the vortex in the layer \mathcal{L}_1 . These waves are not present in the symmetry plane $\mathcal{L}_{1/2}$ (Fig. 14b). The waves were appearing in Fig. 13 as a wiggling of the total density contours away from the vortex centers. The production of these waves and the vertical propagation of the shear layer during the pairing may also explain why the Richardson number does not drop below $1/4$ even for extremely large buoyancy Reynolds number.

7. Conclusion

The merging of two co-rotating columnar vertical vortices in a strongly stratified flow is induced by the development of the zigzag instability. The zigzag instability displaces the vortices closer together (layer \mathcal{L}_1) and farther apart (layer $\mathcal{L}_{1/2}$) alternately every half a wavelength in the vertical direction. The merging occurs first in the layer \mathcal{L}_1 at a time t_1 which is only a function of the initial perturbation and the instability growth rate. The instability literally pushes the vortices together until they merge.

We have observed that the pairing is nearly simultaneous in the whole layer \mathcal{L}_1 . Once the pairing is completed in \mathcal{L}_1 , an intense shear appears between the layers \mathcal{L}_1 and $\mathcal{L}_{1/2}$ where vortices were initially moving apart. This intense vertical shear dissipates energy till the pairing is completed in layer $\mathcal{L}_{1/2}$. The precise mechanism governing the propagation of the pairing on the vertical is complex and not fully unraveled, it seems to be mediated by emission

of internal gravity waves visible in intermediate layers (Fig. 14). Therefore, pairing of tall vortices in a stratified fluid is different from the 2D case: it occurs faster on a time independent of the Reynolds number and a fraction close to 20% of the energy is lost via an energy cascade associated with the generation of small vertical scales of intense shear. If stratified turbulence were associated with pairing events as in 2D turbulence, this loss of energy would reduce the upscale energy cascade and a fraction of the initial energy would cascade towards small vertical scales.

Acknowledgments

We wish to thank gratefully Daniel Guy for technical assistance and Geert Brethouwer for his careful reading of an early draft of this manuscript. This work is supported by IDRIS (CNRS) for computational facilities under project No. 41722.

References

- [1] J.J. Riley, M.P. Lelong, Fluid motions in the presence of strong stable stratification, *Annu. Rev. Fluid Mech.* 32 (2000) 617–657.
- [2] G.D. Nastrom, K.S. Gage, W.H. Jasperson, Kinetic energy spectrum of large- and mesoscale atmospheric processes, *Nature* 310 (1984) 36–38.
- [3] D.K. Lilly, Stratified turbulence and the mesoscale variability of the atmosphere, *J. Atmospheric Sci.* 40 (1983) 749–761.
- [4] R.H. Kraichnan, Inertial ranges in two-dimensional turbulence, *Phys. Fluids* 10 (1967) 1417–1423.
- [5] G.F. Carnevale, J.C. McWilliams, Y. Pomeau, J.B. Weiss, W.R. Young, Evolution of vortex statistics in two-dimensional turbulence, *Phys. Rev. Lett.* 66 (1991) 2735–2737.
- [6] F.S. Godeferd, C. Cambon, Detailed investigation of energy transfers in homogeneous stratified turbulence, *Phys. Fluids* 6 (1994) 2084–2100.
- [7] E. Lindborg, Can the atmospheric kinetic energy spectrum be explained by two-dimensional turbulence? *J. Fluid Mech.* 388 (1999) 259–288.
- [8] J.J. Riley, S.M. de Bruyn Kops, Dynamics of turbulence strongly influenced by buoyancy, *Phys. Fluids* 15 (2003) 2047–2059.
- [9] M.L. Waite, P. Bartello, Stratified turbulence dominated by vortical motion, *J. Fluid Mech.* 517 (2004) 281–308.
- [10] J.J. Riley, E. Lindborg, Stratified turbulence: a possible interpretation of some geophysical turbulence measurements, *J. Atmos. Sci.* 65 (2008) 2416–2424.
- [11] P. Billant, J.M. Chomaz, Theoretical analysis of the zigzag instability of a vertical columnar vortex pair in a strongly stratified fluid, *J. Fluid Mech.* 419 (2000) 29–63.
- [12] P. Otheguy, P. Billant, J.M. Chomaz, Theoretical analysis of the zigzag instability of a vertical co-rotating vortex pair in a stratified fluid, *J. Fluid Mech.* 584 (2007) 103–124.
- [13] P. Otheguy, J.M. Chomaz, P. Billant, Elliptic and zigzag instabilities on co-rotating vortices in a stratified fluid, *J. Fluid Mech.* 553 (2006) 253–272.
- [14] F. Gallaire, J.M. Chomaz, Mode selection in swirling jets: an experimentally based instability analysis, *J. Fluid Mech.* 494 (2003) 223–253.
- [15] D.V. Moore, P. Saffman, The instability of a straight vortex filament in a strain field, *Proc. R. Soc. Lond.* 346 (1975) 413–425.

- [16] H.K. Moffatt, S. Kida, K. Ohkitani, Stretched vortices—the sinews of turbulence—large Reynolds number asymptotics, *J. Fluid Mech.* 259 (1994) 241–264.
- [17] C. Eloy, S. Le Dizès, Three-dimensional instability of Burgers and Lamb–Oseen vortices in a strain field, *J. Fluid Mech.* 378 (1999) 145–166.
- [18] S. Le Dizès, F. Laporte, Theoretical predictions for the elliptical instability in a two-vortex flow, *J. Fluid Mech.* 471 (2002) 169–201.
- [19] M.V. Melander, N.J. Zabusky, J.C. McWilliams, Symmetric vortex merger in two-dimensions: causes and conditions, *J. Fluid Mech.* 195 (1988) 303–340.
- [20] S. Le Dizès, A. Verga, Viscous interaction of two co-rotating vortices before merging, *J. Fluid Mech.* 467 (2002) 389–410.
- [21] P. Meunier, U. Ehrenstein, T. Leweke, M. Rossi, A merging criterion for two-dimensional co-rotating vortices, *Phys. Fluids* 14 (2002) 2757–2766.
- [22] C. Cerretelli, C.H.K. Williamson, The physical mechanism for vortex merging, *J. Fluid Mech.* 475 (2003) 41–77.
- [23] G.K. Batchelor, *An Introduction to Fluid Dynamics*, Cambridge University Press, 1967.
- [24] A. Deloncle, P. Billant, J.M. Chomaz, Nonlinear evolution of the zigzag instability in stratified fluids: a shortcut on the route to dissipation, *J. Fluid Mech.* 599 (2008) 229–239.
- [25] M.L. Waite, P.K. Smolarkiewicz, Instability and breakdown of a vertical vortex pair in a strongly stratified fluid, *J. Fluid Mech.* 606 (2008) 239–273.
- [26] P. Augier, P. Billant, Onset of secondary instabilities on the zigzag instability in stratified fluids, *J. Fluid Mech.* 662 (2011) 120–131.
- [27] P. Augier, J.M. Chomaz, P. Billant, Spectral analysis of the transition to turbulence from a dipole in stratified fluids, *J. Fluid Mech.* 713 (2012) 86–108.
- [28] J.W. Miles, On the stability of heterogeneous shear flows, *J. Fluid Mech.* 10 (1961) 496–508.
- [29] L.N. Howard, Note on a paper of John W. Miles, *J. Fluid Mech.* 10 (1961) 509–512.